

# Selecting Supersymmetric String Scenarios From Sparticle Spectra

---

**B.C. Allanach<sup>1</sup>, D. Grellscheid<sup>2</sup>, F. Quevedo<sup>2</sup>**

<sup>1</sup> *CERN Theory Division, CH-1211 Geneva 23, Switzerland*

<sup>2</sup> *DAMTP, CMS, Wilberforce Road, Cambridge CB3 0WA, UK*

**ABSTRACT:** We approach the following question: if supersymmetry is discovered, how can we select among different supersymmetric extensions of the Standard Model? In particular, we perform an analysis of the sparticle spectrum in low-energy string effective theories, asking which observables best distinguish various scenarios. We examine scenarios differing by the fundamental string scale and concentrate on GUT and intermediate scale models. We scan over all parameters (two goldstino angles,  $\tan\beta$  and the gravitino mass) in each scenario, finding ratios of sparticle masses that provide the maximum discrimination between them. The necessary accuracy for discrimination is determined in each case. We find that the required accuracy on various sparticle mass ratios is at the few percent level, a precision that may be achieved in future linear colliders. We place phenomenological constraints on the parameter space and determine the supersymmetric contribution to the muon anomalous magnetic moment.

**KEYWORDS:** Supersymmetry Breaking, Beyond Standard Model, Supersymmetric Models.

---

## Contents

<b>1. Introduction</b>	<b>1</b>
<b>2. Soft SUSY Breaking Terms</b>	<b>3</b>
2.1 Scalar masses	4
2.2 Gaugino masses	5
2.3 A-terms	5
<b>3. Renormalization Group Analysis</b>	<b>5</b>
3.1 Constraints	6
3.2 String scale boundary conditions	6
3.3 Sparticle spectra	7
3.4 Maps of parameter space	10
3.5 Discriminating ratios	13
3.6 Interpretation	17
<b>4. Conclusions</b>	<b>20</b>

---

## 1. Introduction

There is great expectation in the high energy physics community of the possibility of discovering evidence of low-energy supersymmetry (SUSY) during the next few years. The smoking-gun signatures of production and detection of super-partners could be observable at the Tevatron, the Large Hadron Collider and a future linear collider facility. If such signatures are detected, we may enter a new era of high energy physics with closer contact between fundamental theory and experiment. Since there are many supersymmetric models, the issue may then turn from discovering SUSY to selecting and eliminating the different supersymmetric models that have been proposed over the years. It is therefore useful to examine ways of comparing the different models. Experiments may start to give us information not only about particle content but also about the mechanism of SUSY breaking and (eventually) the messenger of this breaking.

Many argue that the best motivated models of low energy SUSY are those that can be derived from string theory. Even though there is a plethora of possible specific string models, we can attempt to perform a fairly model independent analysis using

some general string scenarios. There are several ways to parameterize these scenarios. In recent years it was realized that the underlying scale of a fundamental string theory can be different from the Planck scale of  $10^{19}$  GeV if the observable fields are confined to a brane within a higher dimensional world. Since the size of the extra dimensions is not necessarily fixed in such a theory, we have the freedom to argue for different values of the string scale. Two such possibilities with several indications in their favour are the GUT scale  $M_{GUT} \sim O(10^{16})$  GeV [1] and the intermediate scale of around  $M_I = 10^{11}$  GeV [2, 3]. The GUT scale is favoured by the data in the MSSM-desert gauge unification picture [1]. The intermediate scale is motivated by a natural solution to the strong CP problem, the scale of neutrino masses [3] and a natural supersymmetry breaking scale in gravity mediated supersymmetry breaking scenarios. But in this case, assuming an MSSM-like low energy spectrum, the gauge couplings evolved from the data at the electroweak scale  $M_Z$  to  $M_I$  do not meet, contrary to the naive string prediction. One must address the issue of gauge unification in the intermediate scale models, and two possibilities have been identified: one possibility is to achieve precocious unification [3] through the inclusion of additional matter fields on top of the MSSM content. Explicit intermediate scale string models have sometimes exhibited the existence of such superfields extra to the MSSM [4]. Another possibility is mirage gauge coupling unification [5]. In this picture, gauge unification at the GUT scale is merely an illusion created by string loop effects; the field theoretic gauge couplings are set non-universally at the (intermediate) string scale. Here, no additional matter fields beyond the MSSM are necessary.

We can imagine having experimental data on supersymmetric particles and would like to see if they may be able to determine the favoured string scale, or other important parameters of the fundamental theory. In this way we would start to obtain relevant information about the fundamental theory at a large scale from measurements at low energies. Motivated by this possibility we ask to what extent we can discriminate scenarios for the underlying theory.

Supersymmetric phenomenology is extremely complicated. The sparticles undergo cascade decays which provide various signatures in experiments. Such signatures notoriously depend not only on the model of SUSY breaking, but also upon its parameters. If a SUSY breaking parameter changes, mass differences in the sparticle spectrum can change sign. Decay channels in the cascade sparticle decays then switch on and off, and the identified signature is easily lost. Such is the complexity of supersymmetric phenomenology that experimental studies of future colliders have typically focused on a few points in parameter space [6].

To avoid getting bogged down in such complexity and model dependence, and in order to start the phenomenology ball rolling, we will assume that some of the superparticles' masses have been measured. We will try to gain information on the high energy theory from their values. Explicitly, we will examine three different

scenarios:

- String scale at the GUT scale  $M_{GUT} \sim O(10^{16})$  GeV, defined by the scale of electroweak gauge unification  $g_1(M_{GUT}) = g_2(M_{GUT})$ .
- Intermediate string scale ( $M_I = 10^{11}$  GeV) with extra leptons to achieve gauge coupling unification at  $M_I$ , which we will refer to as *early unification*.
- Intermediate string scale ( $M_I = 10^{11}$  GeV) with *mirage unification* [5]. The particle spectrum is assumed to be as in the MSSM, and the gauge couplings at  $M_I$  are unequal.

To predict sparticle masses from these scenarios, we must solve the renormalization group equations starting from a theoretical boundary condition parameterized by the string scale, the goldstino angles,  $\tan\beta$  and the gravitino mass  $m_{3/2}$ . Constraints from experiments and cosmology (if a version of  $R$ -parity is conserved, as assumed here) restrict the models.

Previous studies have been performed on intermediate string-type scenarios. Two of the authors [7] previously mapped out the spectrum and naturalness parameter for the dilaton dominated scenario in the GUT, early unification and mirage scenarios. Baek *et al* extended this study to include bounds from  $B \rightarrow X_s\gamma$ , dark matter and  $g-2$  of the muon [8]. The early unification spectrum and relic neutralino density has also been investigated [9] when one of the goldstino angles varies. However, the effects of moduli fields on the SUSY breaking was neglected in this study. Dark matter observables were also considered for mirage or early unification scenarios in ref. [10]. Dilaton domination (corresponding to a fixed limit of one of the goldstino angles) is in violation of a charge and colour breaking bound for GUT scale unification [11], but it was found that this bound does not restrict the intermediate scale case [7].

Here we extend previous investigations in three directions. Firstly, we scan over both of the goldstino angles. Secondly, we look for the combinations of sparticle mass measurements which provide the most discrimination between the string scenarios, once parameters are scanned over. Thirdly, we approach the question: is it possible to select a string scenario from a knowledge of the masses of the different sparticles? We re-phrase this question as: what accuracy in sparticle mass measurements is required to select a string scenario?

## 2. Soft SUSY Breaking Terms

The Type I string models considered here are based on orientifold compactifications of type IIB strings, and share a number of similarities with the well studied phenomenological models derived from compactified heterotic string theories [12]. Both contain a dilaton superfield  $S$ , and moduli fields  $T_i$  connected with the size and shape

of the extra dimensions. These two fields contribute to SUSY breaking when their auxiliary fields acquire vacuum expectation values (VEVs). We consider one overall modulus  $T$  and later one blowing-up mode  $M$  as a parameterization of the stringy SUSY breaking. The respective contribution of  $F^S$  and  $F^T$  to the SUSY soft breaking terms can be parameterized in a goldstino angle  $\theta$  (where  $\sin \theta = 1$  corresponds to dilaton domination and  $\cos \theta = 1$  denotes moduli domination).

One difference between heterotic and type I string models is that the string scale is not constrained to be near the Planck mass. Furthermore, the set of moduli fields connected to the blowing-up modes,  $M_\alpha$ , play a more relevant role for SUSY breaking in Type I models than in the heterotic ones. They contribute explicitly to the gauge kinetic coupling and therefore their  $F$ -terms may induce gaugino masses and the other soft breaking terms.  $M$  mixes in the Kähler potential with the modulus field  $T$ . Accordingly it is convenient to introduce a second,  $(F^T, F^M)$  mixing angle  $\phi$  in analogy to the usual dilaton-moduli mixing angle  $\theta$ . To summarize,

$$\begin{pmatrix} F^S \\ F^T \\ F^M \end{pmatrix} = \begin{pmatrix} \sin \theta \\ \cos \theta \sin \phi \\ \cos \theta \cos \phi \end{pmatrix} F_{total}, \quad (2.1)$$

where  $F_{total} = \sqrt{F_S^2 + F_T^2 + F_M^2}$ .

The introduction of  $\theta$  and  $\phi$  provides a convenient way to parameterize the influence which the various VEVs have on the soft terms. We will generalize the results of ref. [7] where only the dilaton domination case was considered extensively. Here, we examine a wider  $\theta$  and  $\phi$  range but leave out  $\theta < 30^\circ$ . For such small values of  $\theta$ , the string-induced high scale boundary conditions on the soft breaking terms are of similar magnitude to the one-loop order anomaly mediated SUSY breaking terms, which therefore cannot be neglected. The complete set of soft breaking terms of combined anomaly and gravity mediation has not yet been computed [13]. We therefore leave this slice of parameter space to the future, when such terms might be included in an analysis. Like the analysis in [7], we assume that the full standard model gauge group arises from a single brane and that SUSY breaking is dominated by the  $F$  terms of the  $S$ ,  $T$  and  $M$  fields. This results in the following soft breaking terms in the  $T + \bar{T} \rightarrow \infty$  limit:

## 2.1 Scalar masses

All scalar masses receive the universal soft SUSY breaking term

$$m_0^2 = V_0 + m_{3/2}^2 \left( 1 - \frac{3}{k} C^2 \cos^2 \theta \sin^2 \phi \right) + \mathcal{O} \left( \frac{1}{(T + \bar{T})^2} \right), \quad (2.2)$$

where  $C = \sqrt{1 + \frac{V_0}{3m_{3/2}^2}}$ , and  $V_0$  is the vacuum energy.  $k$  depends on the form of the Kähler potential and can be set constant [7]. We set  $k = 3$  in this article, which

avoids negative scalar mass squared values at the string scale. Higher values of  $k$  are possible, this would lead to a weaker dependence of the scalar soft masses on the goldstino angles. As usual we will take  $C = 1$  corresponding to  $V_0 = 0$ , *i.e.* a vanishing cosmological constant.

## 2.2 Gaugino masses

The gaugino masses are equal to

$$M_a = \sqrt{3}Cm_{3/2} \frac{\alpha_a}{\alpha_{\text{GUT}}} \left( \sin \theta - \frac{s_a}{8\pi} \alpha_{\text{GUT}} \cos \theta \left( \frac{\delta_{\text{GS}}}{\sqrt{k}} \sin \phi + \cos \phi \right) \right) + \mathcal{O} \left( \frac{1}{(T + \bar{T})^2} \right). \quad (2.3)$$

Here  $\delta_{\text{GS}}$  is the Green-Schwarz term coming from anomaly cancellation (like in compactified heterotic string models). Its value is a model dependent negative integer of order  $\mathcal{O}(-10)$ . We will fix its value to  $-10$  from here on (our results are not substantially modified by varying  $\delta_{\text{GS}}$ ). Note that, in general, the gaugino masses have a non-universal boundary condition at the string scale. If the string scale is intermediate,  $\alpha_{a=1,2,3} \neq \alpha_{\text{GUT}}$  provides non-universality in equation (2.3) from the first term. The second term provides non-universality at the string-scale through one-loop stringy effects away from the dilaton dominated limit ( $\theta = 90^\circ$ ). This term is proportional to the model-dependent parameters  $s_a$ . In order to make mirage unification possible,  $s_a = 2\pi\beta_a$  was chosen [5], where  $\beta_a$  are the usual MSSM renormalization  $\beta$ -function coefficients  $(33/5, 1, -3)$ .

## 2.3 A-terms

Under the assumption that the Yukawa couplings are moduli-independent, the trilinear couplings are

$$A_{\alpha\beta\gamma} = -\sqrt{3}Cm_{3/2} \left( \sin \theta + \cos \theta \cos \phi \hat{K}' \right) + \mathcal{O} \left( \frac{1}{(T + \bar{T})^2} \right). \quad (2.4)$$

Here  $\hat{K} = \hat{K}(M + M^* - \delta_{\text{GS}} \log(T + T^*))$ , the  $M$ - and  $T$ -dependent part of the Kähler potential. One can set  $\hat{K}' = 0$  [7], since all fields are assumed to be in the minimum of the potential, for which the argument of  $\hat{K}$  vanishes.

## 3. Renormalization Group Analysis

In order to analyze the sparticle spectra we use the ISASUGRA part of the ISAJET 7.51 package [14] to obtain the SUSY spectrum starting from the high-energy boundary conditions detailed above.

### 3.1 Constraints

We use the following experimental constraints to limit the scenarios [15]:

$$m_{\tilde{\chi}_1^0} > 32.3 \text{ GeV} \quad m_{\tilde{\chi}_1^\pm} > 67.7 \text{ GeV} \quad m_{h_0} > 113.5 \text{ GeV} \quad (3.1)$$

These are the most restrictive general mass bounds upon the scenarios we study.

We will also use constraints from the recently measured muon anomalous magnetic moment  $a_\mu = (g - 2)/2$ . The experiment E821 at Brookhaven National Laboratory (BNL) reported the measurement [16]

$$a_\mu = (11659202 \pm 14 \pm 6) \times 10^{-10}, \quad (3.2)$$

which differs from the Standard Model prediction by

$$\delta a_\mu = (43 \pm 16) \times 10^{-10}, \quad (3.3)$$

a  $2.6\sigma$  deviation. This may be a signal of new physics beyond the Standard Model [17], and supersymmetric models can provide the necessary extra contribution [18]. At the moment, we can use this discrepancy only with some caution because it is only a  $2.6\sigma$  deviation and because there may yet be unresolved systematics in the higher order corrections used to derive it from the experimental results. The precision in the measurement already significantly constrains the SUSY parameter space and will improve in the future. We will constrain all investigated models to be within  $2\sigma$  of the central value of the measurement, *i.e.*

$$11 \times 10^{-10} < \delta a_\mu < 75 \times 10^{-10}. \quad (3.4)$$

The final constraint is the absence of a charged lightest supersymmetric particle (CLSP). This constraint must be applied because we implicitly assume that a version of  $R$ -parity holds, as recently found in specific string models [19].

### 3.2 String scale boundary conditions

As mentioned above, we consider three overall scenarios: GUT scale unification (with the string scale set to  $M_S = 2 \times 10^{16}$  GeV), early unification and mirage unification (both with  $M_S = M_I = 1 \times 10^{11}$  GeV). The MSSM spectrum is assumed in each case, except for early unification where  $2 \times L_L + 3 \times E_R$  vector-like representations are added to the MSSM in order to achieve gauge unification at  $M_I$  [7]. It is assumed that these extra representations have negligible Yukawa couplings. We add their effect to the MSSM gauge  $\beta$ -functions above 1 TeV.

The string-scale boundary condition on the soft terms were obtained from equations (2.2-2.4), with  $m_{3/2}$ ,  $\theta$  and  $\phi$ , as well as  $\tan \beta$  as free parameters. Throughout the whole analysis  $\mu > 0$  and  $m_t = 175$  GeV were assumed [15]. In the GUT case,  $\alpha_a = \alpha_{\text{GUT}} = 1/25$  was used in equation (2.3) for all gauge groups  $a = 1, 2, 3$ . In

	$\theta$	$\phi$	$m_{3/2}$	$\tan\beta$	$\mu$	$m_t$	$V_0$	$C$	$k$	$\delta_{GS}$	$M_{GUT}$	$M_I$
range	30-90°	0-90°	50-1500	2-50	> 0	175	0	1	3	-10	$2 \times 10^{16}$	$10^{11}$
step	10°	10°	50	2								

**Table 1:** Summary of parameters. The first four parameters are scanned over, and their range and increment are detailed. For the others with no ‘step’ entry, their value is kept constant except for  $\mu$  which is constrained to give the correct value of  $M_Z$ . All massive parameters ( $m_{3/2}, m_t, M_I, M_{GUT}$ ) are given in units of GeV.

the mirage unification case, however, the gauge couplings only *appear* to unify at the GUT scale. In reality they are set at the intermediate scale  $M_I = 10^{11}$  GeV to non-universal values<sup>1</sup>. In our analysis,

$$\alpha_1(M_I) = \frac{1}{37.6}, \quad \alpha_2(M_I) = \frac{1}{27.0}, \quad \alpha_3(M_I) = \frac{1}{19.8} \quad (3.5)$$

is the set of values which remains stable under iterations of inserting them into equation (2.3) and running the RGEs again.

For each of the three scenarios that we consider, we scan over the free parameters  $\theta$ ,  $\phi$ ,  $\tan\beta$  and  $m_{3/2}$ .  $\theta = 90^\circ$  corresponds to the dilaton domination case considered in [7], and the SUSY soft mass terms are independent of  $\phi$  in this case. As mentioned above, values of  $\theta < 30^\circ$  were not considered, since in this case tree level soft masses would vanish and it would not be possible to neglect the one-loop effects from anomaly mediated SUSY breaking, which might modify the soft terms considerably. Table 1 shows the ranges and increments of scanned parameters. It also summarizes the other parameters that were kept constant.

### 3.3 Sparticle spectra

In order to get some feeling for the effect of the goldstino angles, we first illustrate their effect upon the sparticle spectra. We choose the mirage unification scenario as a first example. The other scenarios do differ from these spectra quantitatively, but the effect of the goldstino angles is similar in each case. In figure 1, we show the variation of the mirage unification spectrum with  $\theta$  for  $\tan\beta = 30$ ,  $m_{3/2} = 300$  GeV and  $\phi = 60^\circ$ . As mentioned above,  $\theta = 90^\circ$  corresponds to the dilaton dominated limit. From the figure, we see that larger  $\theta$  increases the splittings between sparticles. Larger  $\theta$  corresponds to larger gaugino masses in eq. (2.3) and the larger gluino mass raises the other coloured sparticle masses in the running from  $M_I$  to  $M_Z$ . The weak gauginos also show a milder change from the larger values of  $M_{1,2}$ . Sleptons are largely unaffected by the variation of  $\theta$ , demonstrating the fact that the mild increase in  $m_0$  in eq. (2.2) from increasing  $\theta$  is a relatively minor effect.

<sup>1</sup>We note that ref. [7] assumes gaugino universality, which leads to different conclusions for the mirage scenario, especially for the charged LSP constraints.



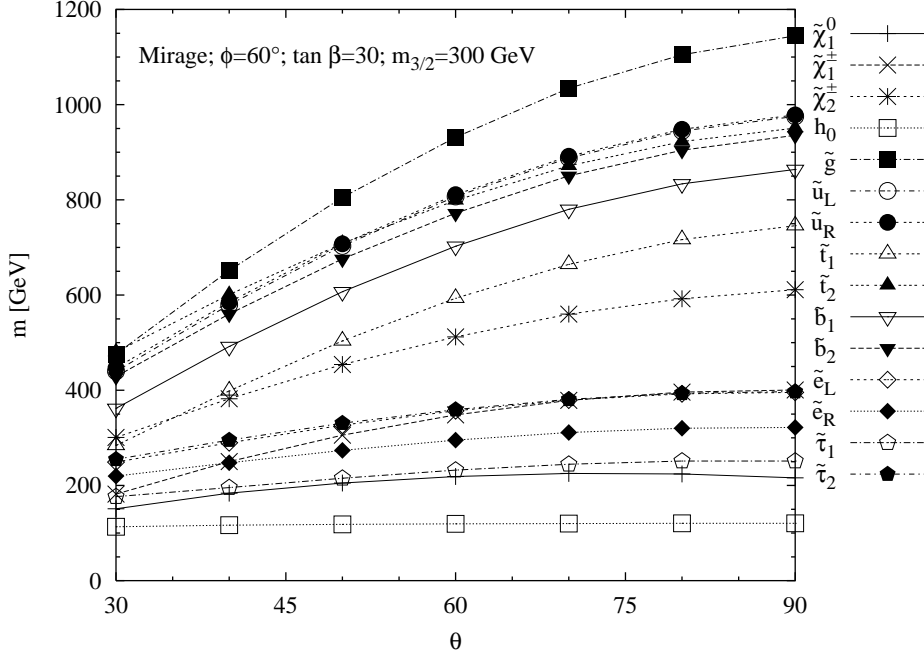
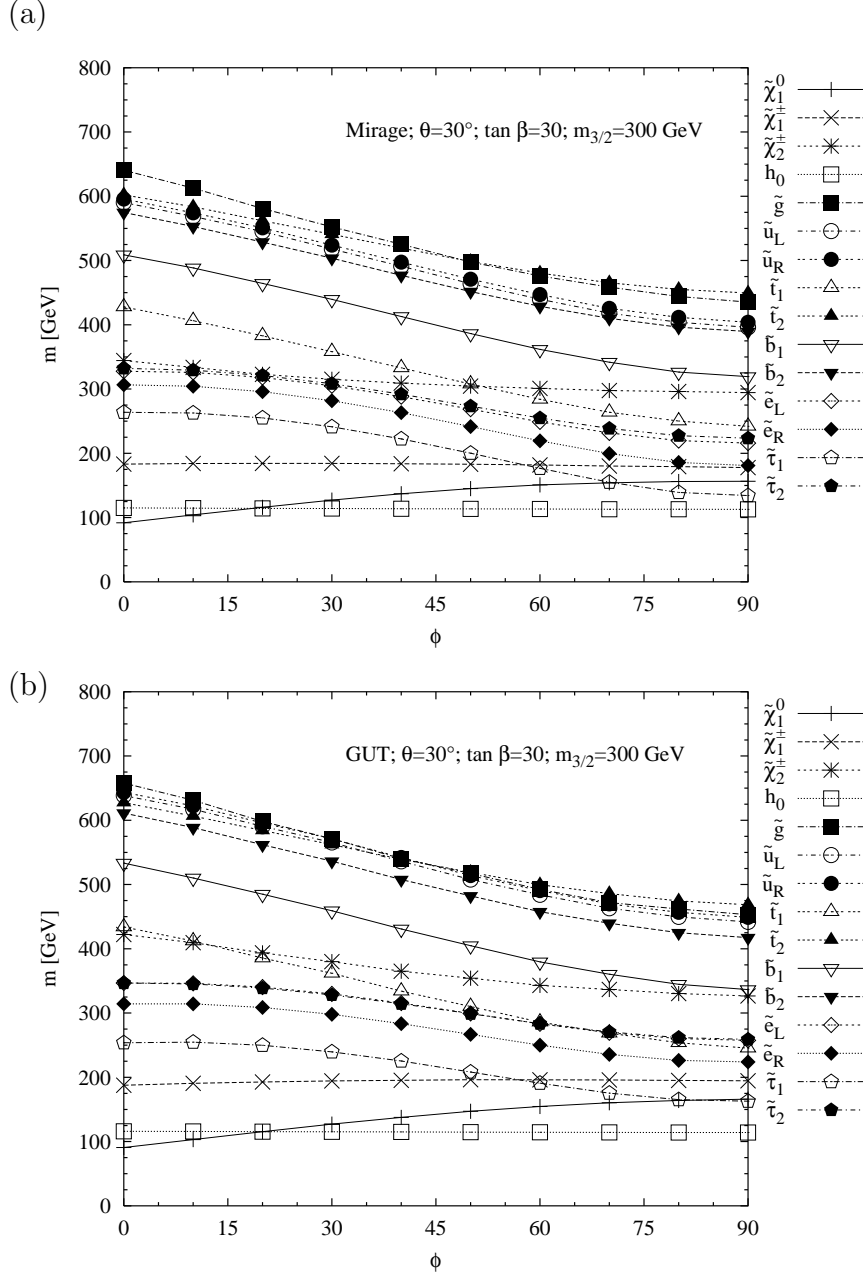


**Figure 1:** Variation of mirage unification sparticle mass spectrum with  $\theta$ . We use  $\phi = 60^\circ$ ,  $\tan \beta = 30$  and  $m_{3/2} = 300$  GeV. The key on the right-hand side of the figure details the flavour of particle.

The ordering of superparticle masses is largely unaffected by changes in  $\theta$ , except for the lightest chargino (which crosses the slepton masses) and the lightest stop which crosses the heavier chargino line. Each ordering will correspond to different cascade decay channels, and might be used to restrict  $\theta$  once these decays are observed.

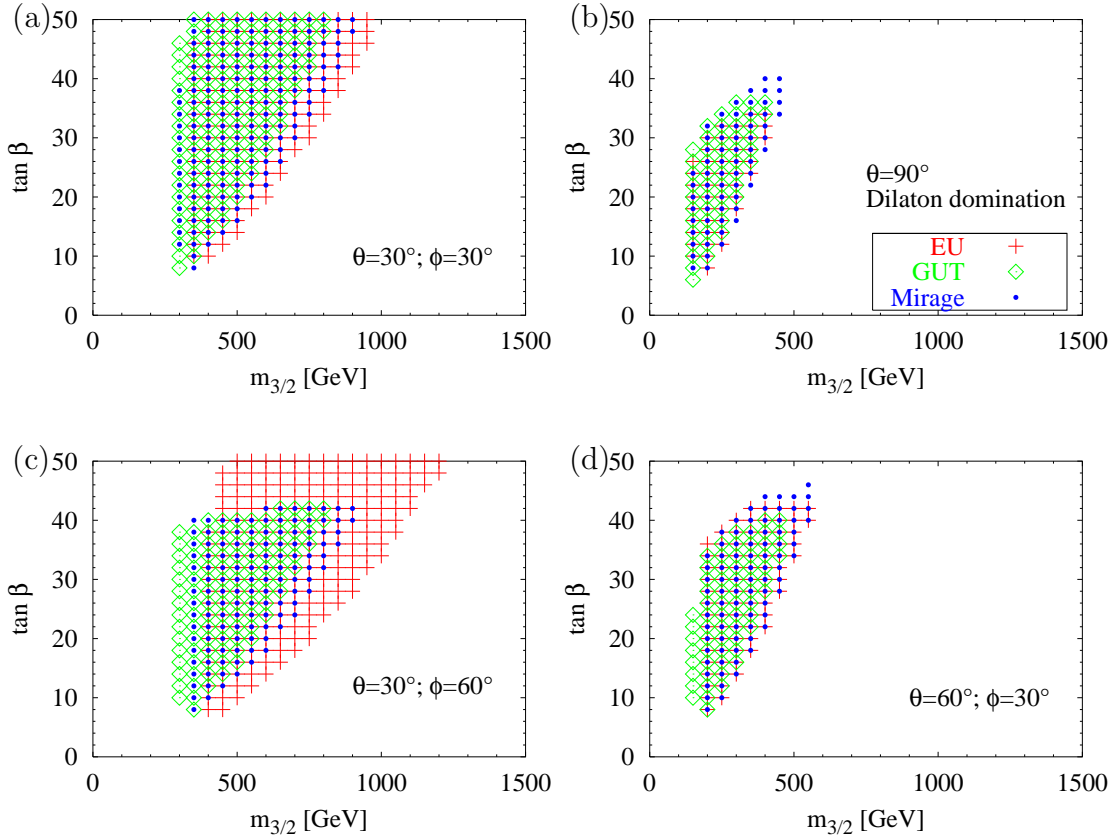
In figure 2a, we show the variation of the mirage unification sparticle spectrum with  $\phi$  for  $\tan \beta = 30$ ,  $m_{3/2} = 300$  GeV and  $\theta = 30^\circ$ . Here, increasing  $\phi$  has a smaller effect than  $\theta$ , but generally decreases the splittings between sparticle masses. The effect is relatively small because the gaugino masses are only sensitive to  $\phi$  through a suppression factor in eq. (2.3). Most of the sparticle masses decrease with increasing  $\phi$ , except for the lightest neutralino (which becomes heavier) and the lightest chargino (which remains roughly constant). This can be understood by considering the effect of increasing  $\phi$  on the scalar masses in eq. (2.2). The figure shows that the model would be ruled out for  $\theta \geq 70^\circ$  because of a stau LSP. Aside from this, important changes in the ordering of sparticle masses occur between the lightest stau and chargino and the heavier chargino and the lightest stop. The heavier stop becomes heavier than the gluino for  $\phi > 50^\circ$ . This is important because future  $e^+e^-$  machines can produce and measure gluinos more easily through the decays of pair-produced squarks.

Figure 2b shows the variation of the GUT scale unification sparticle spectrum



**Figure 2:** Variation of sparticle mass spectrum with  $\phi$  for (a) mirage and (b) GUT-scale unification scenarios. We use  $\theta = 30^\circ$ ,  $\tan\beta = 30$  and  $m_{3/2} = 300$  GeV. The key on the right-hand side of the figure details the flavour of sparticle.

with  $\phi$  for  $\tan\beta = 30$ ,  $m_{3/2} = 300$  GeV and  $\theta = 30^\circ$ . While quantitative differences exist between figures 2a and 2b, it is clear that the two spectra are qualitatively very similar. There is, however, some re-ordering of sparticle masses between the GUT-scale and mirage-scale scenarios for certain values of  $\phi$ . For example, at  $\phi = 20^\circ$ , the heavy chargino and light stop are interchanged. It would be difficult to discriminate the two scenarios on the basis of decays implying a certain ordering of



**Figure 3:** Maps of parameter space for the early unification (red crosses), mirage (blue dots) and GUT unification scale (green diamonds) scenarios. Here, we plot viable regions of  $\tan\beta$ - $m_{3/2}$  parameter space for fixed values of the goldstino angles: (a)  $\theta = 30^\circ$ ,  $\phi = 30^\circ$ , (b)  $\theta = 90^\circ$ ,  $\phi = \text{arbitrary}$ , (c)  $\theta = 30^\circ$ ,  $\phi = 60^\circ$ , (d)  $\theta = 60^\circ$ ,  $\phi = 30^\circ$ .

the lightest stop and chargino since there is no *a priori* information about  $\phi$ , although it might be possible to fit the masses to certain values of  $\theta, \phi$  if the experimental accuracy were good enough. For larger values of  $\theta$ , the variation of the spectrum with  $\phi$  significantly decreases because the terms that depend upon it in the boundary conditions eqs. (2.2)-(2.4) become smaller and sub-dominant to the other  $\theta$  dependent terms. We have explicitly checked that this is indeed the case. For example, at  $\theta = 60^\circ$ , the maximum variation due to  $\phi$  is a 20% change (in the gluino mass) for mirage *or* GUT-scale unification.

### 3.4 Maps of parameter space

We now explore the parameter space, including constraints from the sparticle mass limits in eq. (3.1), requiring that the  $g-2$  anomalous magnetic moment be within  $2\sigma$  of the central measured value, requiring correct electroweak symmetry breaking and imposing a neutral LSP. In figure 3, we present viable regions of  $\tan\beta$ - $m_{3/2}$  parameter space for various points in the goldstino angle space. Dilaton domination has been

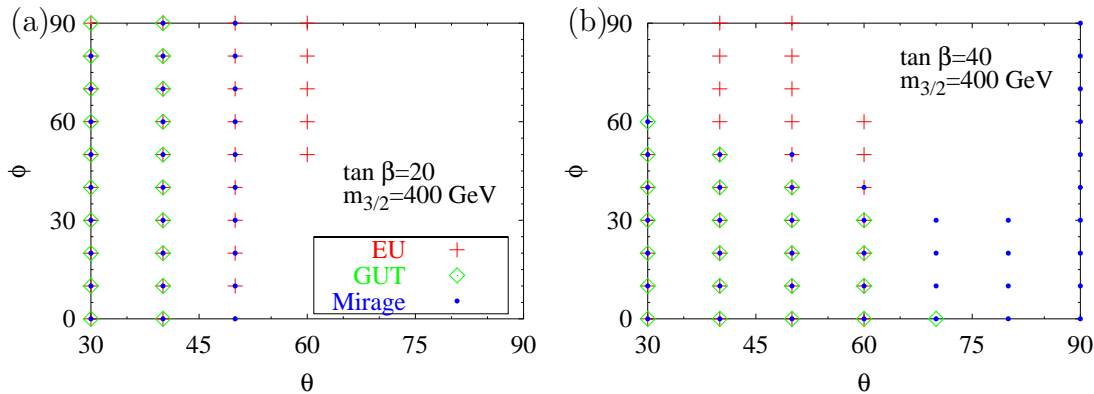


**Figure 4:** Maps of parameter space for the early unification (red crosses), mirage (blue dots) and GUT unification scale (green diamonds) scenarios. Here, we plot viable regions of  $\theta$ - $\phi$  parameter space for fixed values of  $m_{3/2}$  and  $\tan \beta$ : (a)  $m_{3/2} = 400$  GeV,  $\tan \beta = 20$ , (b)  $m_{3/2} = 400$  GeV,  $\tan \beta = 40$

well covered in the literature [7, 8] and so we present other more general regions of the parameter space alongside the dilaton dominated limit in figure 3b. The figure illustrates the fact that the viable parameter space extends to high  $m_{3/2}$  only for high  $\tan \beta$ . This is because the SUSY contribution to  $g - 2$  is roughly proportional to  $\tan \beta$  and inversely proportional to the square of  $m_{3/2}$  (the SUSY particle mass scale) [18]. We see from the variation in the viable regions from figures 3a-3d that they are crucially dependent upon the goldstino angles, which vary between each of the figures.

The main reason for the rapidly varying allowed region is the  $g-2$  limit. As a rule of thumb, the lower the angles are, the larger the allowed region can be, because the sparticles are lighter. We can see that in most cases there is a maximum possible value for the gravitino mass. For small  $\theta = 30^\circ$  (as in figure 3a),  $\tan \beta$  is not limited within the studied range ( $\tan \beta < 50$ ) and in particular the early unification scenario tends to allow larger possible values of the gravitino mass for a given  $\tan \beta$ . Early unification is less constrained, except near the dilaton dominated limit shown in figure 3b. The mirage and GUT-scale unification scenarios have more similar viable regions. The three scenarios overlap substantially, all giving a limited allowed range for the gravitino mass and  $\tan \beta$ . It is interesting that there is often a completely bounded viable region, for example the dilaton-dominated limit shown in figure 3b and  $\theta = 60^\circ, \phi = 30^\circ$  in figure 3d. This implies that for these specific values of goldstino angles, there are upper bounds upon the sparticle masses, translating into an upper bound upon  $m_{3/2}$ . This results of course from the  $g - 2$  limits. For sparticles that are too heavy, one receives no supersymmetric contribution to  $g - 2$ . There are often also bounds upon  $\tan \beta$ . Low  $\tan \beta$  is ruled out by the direct lower bound upon the Higgs mass from LEP2 [15], whereas high  $\tan \beta$  is either ruled out by the

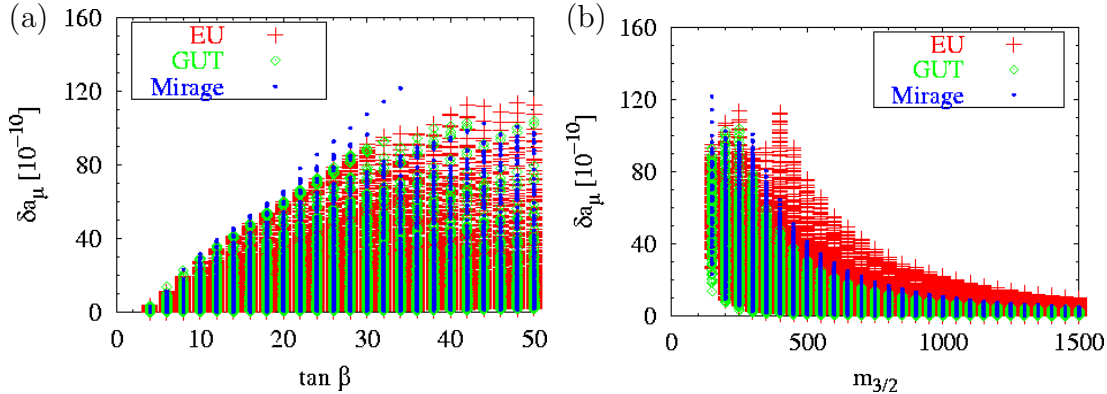


**Figure 5:** Possible values of  $\delta a_\mu$  in the three scenarios as a function of (a)  $\tan\beta$  and (b)  $m_{3/2}$ .  $g-2$  constraints have not been applied. The maximal value of  $\delta a_\mu$  depends strongly on the higgs mass cutoff used. A cutoff of 117 GeV leads to maximal values of around 70 instead of 120.

constraint of a neutral LSP, or of not too *large* a supersymmetric contribution to  $g-2$  of the muon. For instance in the dilaton domination case we can see that the GUT scale scenario restricts  $\tan\beta < 40$ , the early unification scenario requires  $\tan\beta < 34$  and mirage unification constrains  $\tan\beta < 36$ . For the lower value of  $\theta = 30^\circ$ , the  $\tan\beta$  bound disappears for  $\phi = 30^\circ$  in all scenarios as in figure 3a, but reappears for higher  $\phi = 60^\circ$  in the mirage and GUT-scale unification scenarios (figure 3c).

Overall, we find completely bounded regions for  $\theta \geq 60^\circ$  in all three scenarios, and additionally for  $30^\circ \leq \theta \leq 50^\circ$  and  $\phi \geq 50^\circ$  in the GUT and Mirage scenarios. The upper bound on  $\tan\beta$  in these regions varies between 20 and 50, the upper bound on  $m_{3/2}$  between 400 and 900 GeV. Outside the mentioned regions, the allowed data points go beyond the investigated parameter space of  $\tan\beta \leq 50$ .

In figures 4a and 4b, we show the viable regions in goldstino angle space for fixed  $m_{3/2} = 400$  GeV and  $\tan\beta = 20, 40$  respectively. We see that there exists an upper bound upon the value of  $\theta$  for these choices. Dilaton domination ( $\theta = 90^\circ$ ) is not viable here except for the mirage case. For the lower value of  $\tan\beta = 20$  in figure 4a,  $\theta \leq (60^\circ, 50^\circ, 40^\circ)$  for early, mirage and GUT-scale unification respectively, whereas for higher  $\tan\beta = 40$  in figure 4b,  $\theta \leq (60^\circ, 90^\circ, 70^\circ)$  respectively. There are no absolute bounds for  $\phi$  for  $\tan\beta = 20$  in any of the scenarios, but  $\phi \leq 60^\circ$  for the GUT case at  $\tan\beta = 40$ . For  $\phi = 0^\circ$ , there is still a large contribution to unification-scale sparticle masses from terms involving  $\theta$ , so a lower bound on  $\phi$  does not exist for general  $\theta$  from sparticle mass bounds. Lower bounds upon  $\theta$  presumably do exist, but as mentioned above, we do not have the technology to calculate them.

Finally in figures 5a-5b we show the muon anomalous magnetic moment against the free variables. The points here have not had the anomalous  $g-2$  constraint applied to them. For all the angles, the figure shows that the maximum value of

$a_\mu$  is around  $120 \times 10^{-10}$  for the early unification and mirage scenarios and around  $100 \times 10^{-10}$  for the GUT scale scenario. If a more stringent higgs mass limit of 117 GeV is applied, these values are reduced to  $70 \times 10^{-10}$  and  $60 \times 10^{-10}$  respectively. The correlation of maximal  $g - 2$  with  $\tan \beta$  is similar in each scenario, but there exist differences when plotted against  $m_{3/2}$ .

### 3.5 Discriminating ratios

We have searched through ratios of masses of sparticles to see which ones provide the largest discrimination between the three scenarios examined. The objective is to find ratios that are predicted to be in completely disjoint regions for the three scenarios. Then, if the mass ratios were determined in an experiment, a comparison with these disjoint regions should reject or confirm one scenario. Here, we will focus on the accuracy required in any mass ratio measurement that would be enough to discriminate the ratio from the other scenarios. This required accuracy then is the minimum distance between the two disjoint regions. One ratio on its own does not provide complete separation once the parameters in each scenario are scanned over; we therefore resort to considering combinations of two ratios in order to see if the regions of each scenario are separated in two dimensional ratio space.

There are a few combinations of ratios that provide near separation. We display the best two such combinations in figure 6. For each point in the parameter scan described in table 1, that satisfies the constraints in eq. (3.1) as well as the neutral LSP constraint, one point appears on the plot. Each of the three scenarios were scanned over and shown on the plots. In figs. 6a,b the  $g - 2$  constraint has not been applied. In figure 6b there is some overlap between the early unification and each of the other two scenarios, but not so in figure 6a, which shows that there is complete discrimination between the mirage and GUT-scale scenarios provided a 5% measurement of  $m_{\tilde{g}}/m_{\tilde{u}_L}$  and a 20% measurement of  $m_{\tilde{d}_L}/m_{\tilde{e}_R}$  can be made. From figure 6b, it is clear that discrimination based on  $m_{\tilde{g}}/m_{\tilde{u}_L}$  and  $m_{\tilde{e}_L}/m_{\tilde{e}_R}$  is harder, requiring about 1% and 5% accuracy in the mass ratios respectively to discriminate the mirage and GUT-scale unification scenarios. Figures 6c,6d show that this situation significantly improves once the  $g - 2$  bounds are imposed, because the viable regions in each plot shrink, making discrimination easier. Although there is still not perfect discrimination in the general scenario, the region of overlap is small. Figure 6c has only one such region at  $m_{\tilde{g}}/m_{\tilde{u}_L} \sim 1.07$  and  $m_{\tilde{d}_L}/m_{\tilde{e}_R} \sim 2$ . Figure 6d displays two such overlap regions at  $(m_{\tilde{g}}/m_{\tilde{u}_L}, m_{\tilde{e}_L}/m_{\tilde{e}_R}) \sim (1.1, 1.05), (1.1, 1.2)$  respectively. If the empirical uncertainties on mass ratios are small enough and the underlying model does not lie in one of these regions, the correct scenario would be selected over the other two.

It is possible that other measurements (for example measuring Higgs couplings) will constrain some of the parameters of the model. For this reason, we will now assume that two of the four variables  $\theta$ ,  $\phi$ ,  $\tan \beta$  or  $m_{3/2}$  are constrained in order to

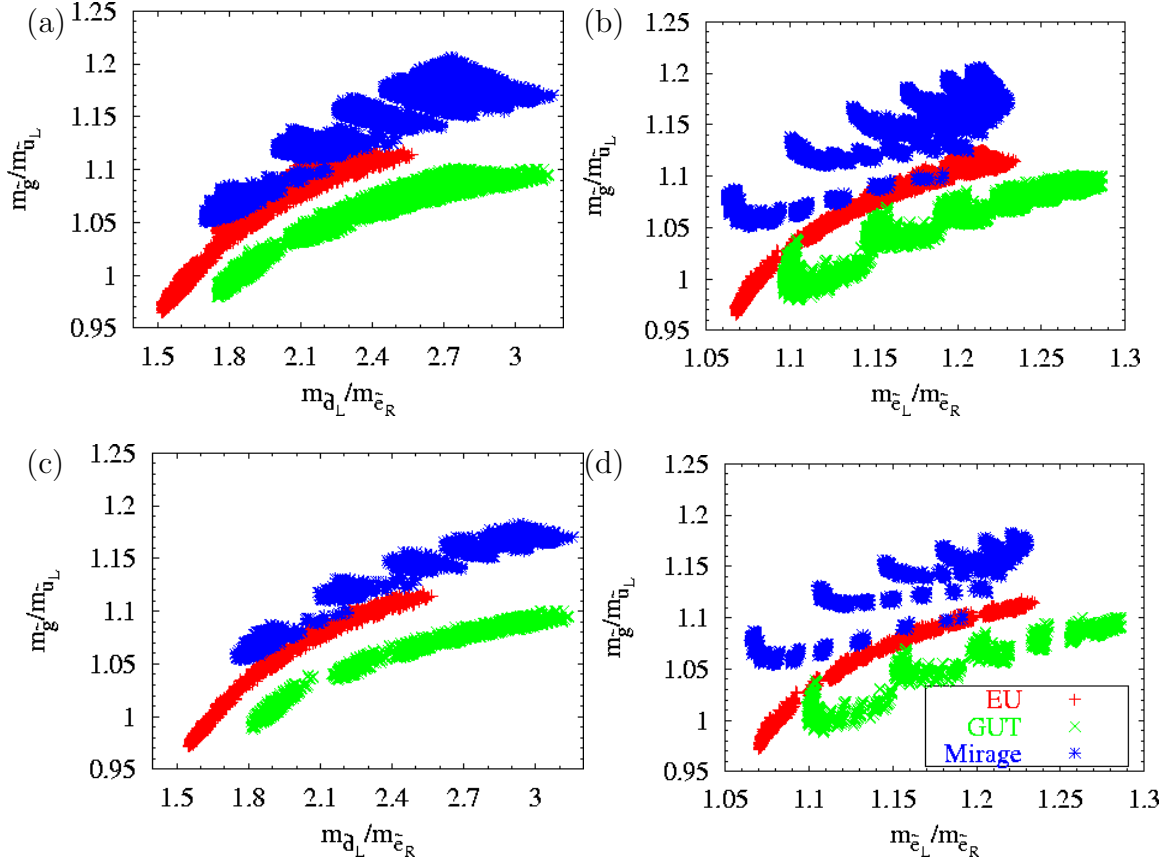


**Figure 6:** Highly discriminating ratios of sparticle masses. Each plotted point corresponds to one data point in four-dimensional parameter space  $(\theta, \phi, \tan\beta, m_{3/2})$  that is not excluded by the imposed limits. Constraints upon the anomalous magnetic moment of the muon have been used in (c),(d) but not in (a),(b). Pluses correspond to the early unification scenario, crosses to GUT-scale unification and stars to mirage unification. The blockiness especially of the GUT and Mirage regions is an artefact of the finite step size used to scan over the goldstino angles.

see the resulting improvement in string scenario discrimination. An obvious example to examine is the dilaton domination scenario (corresponding to  $\theta = 90^\circ$ ), which has attracted attention in the past in its own right. In figure 7, we plot the ratios of masses  $x \equiv m_{\tilde{e}_L}/m_{\tilde{e}_R}$  against  $y \equiv m_{\tilde{g}}/m_{\tilde{u}_L}$  in the dilaton domination limit for all scanned values of the gravitino mass and  $\tan\beta$  in table 1. We can clearly distinguish between the three scenarios because there is no overlap in their regions in ratio parameter space. From the figure, we note that at least a 6% measurement of  $m_{\tilde{g}}/m_{\tilde{u}_L}$  and a 5% measurement in  $m_{\tilde{e}_L}/m_{\tilde{e}_R}$  would be required to separate the models on the basis of these ratios alone. We can see from the figure that applying the  $2\sigma$   $g - 2$  muon anomalous magnetic moment constraints makes the region occupied by each scenario smaller, providing better discrimination between them. This is a very

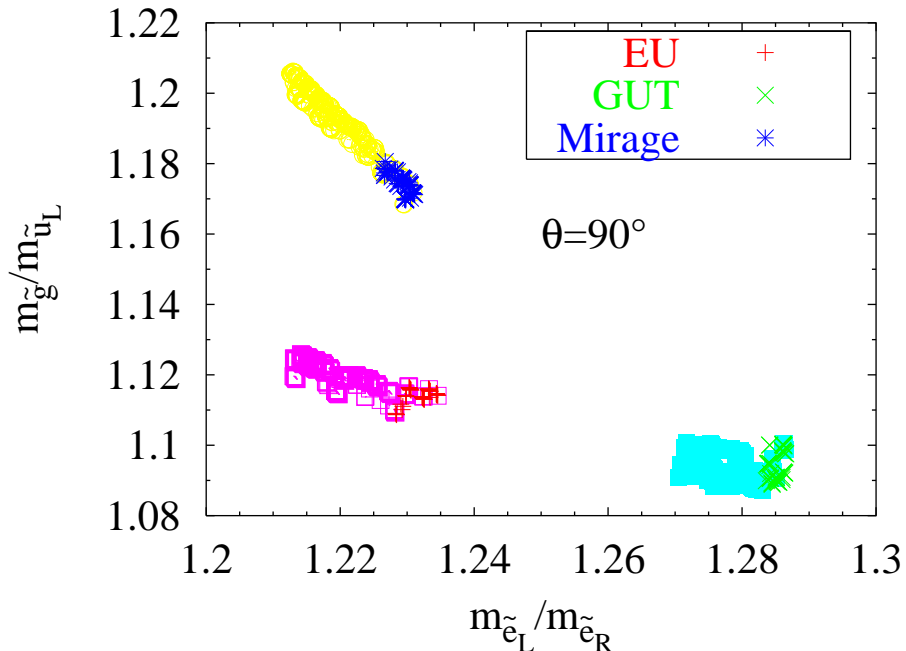


**Figure 7:** Highly discriminating ratios of sparticle masses for dilaton domination ( $\theta = 90^\circ$ ). Each plotted point corresponds to one  $(m_{3/2}, \tan \beta)$ -pair in the scan not excluded by any limits. Green crosses are predicted by the GUT unification scale, early unification is denoted by red crosses, and blue stars are valid for the mirage unification scenario.  $g - 2$  limits have not been applied to the yellow circles (mirage unification), purple squares (early unification) and cyan squares (GUT-scale unification).

positive result: assuming dilaton domination, complete discrimination is possible. If the  $g - 2$  constraints are not applied, we still have complete discrimination, although the required measurement accuracy upon mass ratios changes  $m_{\tilde{e}_L}/m_{\tilde{e}_R}$  would need to be measured to higher accuracy (3.5%).

Departing from dilaton domination complicates the situation considerably, and such a clear and simple separation can no longer be made by using these ratios. Figure 8 illustrates a departure from dilaton domination.  $m_{3/2}$  and  $\tan \beta$  have been fixed in the figure, whereas  $\theta$  and  $\phi$  have been scanned over as in table 1. The figure shows the variation of the ratios  $m_{\tilde{e}_R}/m_{\tilde{g}}$  and  $m_{\tilde{u}_L}/m_{\tilde{g}}$  as well as the variation of  $m_{H^0}/m_{\tilde{b}_2}$  and  $m_{A^0}/m_{\tilde{t}_2}$  with string scenario. The figure again shows that it is easier to distinguish between the mirage and GUT-scale unification scenarios than between either of these and the early unification scenario by using mass ratios. Figures 8a and 8b have  $\tan \beta = 30$  and  $m_{3/2} = 250$  GeV fixed to different values than figures 8c and 8d ( $\tan \beta = 6$  and  $m_{3/2} = 200$  GeV), in order to illustrate how the required discrimination accuracy can depend upon the constrained parameters. Discrimination is shown to generally be achieved for errors smaller than 2% in  $m_{\tilde{e}_R}/m_{\tilde{g}}$  and  $m_{\tilde{u}_L}/m_{\tilde{g}}$  in the mass ratios from figure 8a. These numbers happen to be roughly



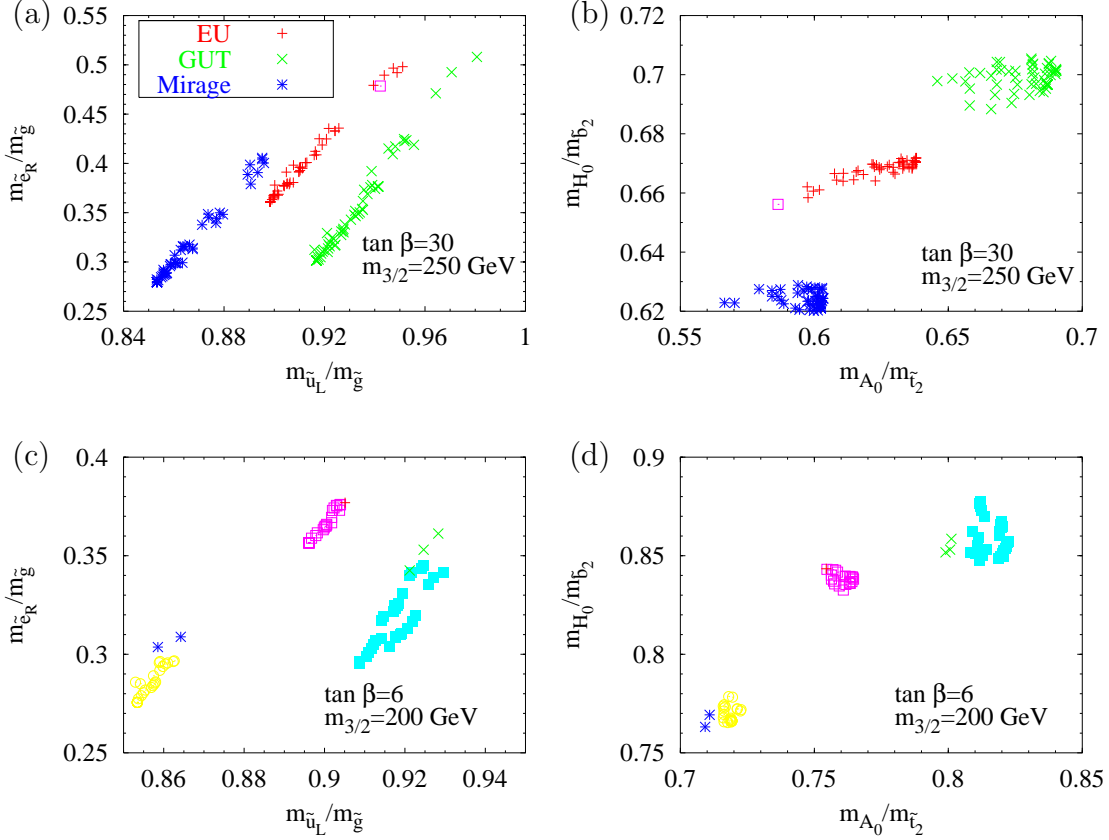


**Figure 8:** Highly discriminating ratios of sparticle masses for (a), (b):  $\tan \beta = 30$ ,  $m_{3/2} = 250$  GeV and (c), (d):  $\tan \beta = 6$ ,  $m_{3/2} = 200$  GeV. Each plotted point corresponds to one  $(\theta, \phi)$ -pair in the scan not excluded by the bounds. Green crosses are predicted by the GUT unification scale, early unification is denoted by red crosses, and blue stars are valid for the mirage unification scenario.  $g - 2$  limits have not been applied to the yellow circles (mirage unification), purple squares (early unification) and cyan squares (GUT-scale unification).

identical for a different choice of  $\tan \beta$  and  $m_{3/2}$ , as shown in figure 8c. However, the accuracy required to discriminate any *two* models changes in the two parameter sets. For example, 2% is the accuracy required to separate the early unification and GUT-scale scenarios for the first set in figure 8a and 5% for the same scenarios in the second set of figure 8c. Also, the inclusion or exclusion of the  $g - 2$  constraint does not have a significant effect for the first choice of parameters, contrary to the case for the second choice of parameters. Figures 8b,d show how discrimination could be achieved with 5% errors on  $m_{H_0}/m_{\tilde{b}_2}$  and  $m_{A_0}/m_{\tilde{t}_2}$ . We note that the overall values of these two ratios in any one scenario depends sensitively upon the values of  $\tan \beta$  and  $m_{3/2}$ .  $\tan \beta$  and  $m_{3/2}$  could then be constrained by their measurement.

We now fix the goldstino angles, to see if it is possible to distinguish the models when they are scanned over  $m_{3/2}$  and  $\tan \beta$ . The usefulness of combinations of ratios of sparticle masses depends in general upon the value of these goldstino angles. As

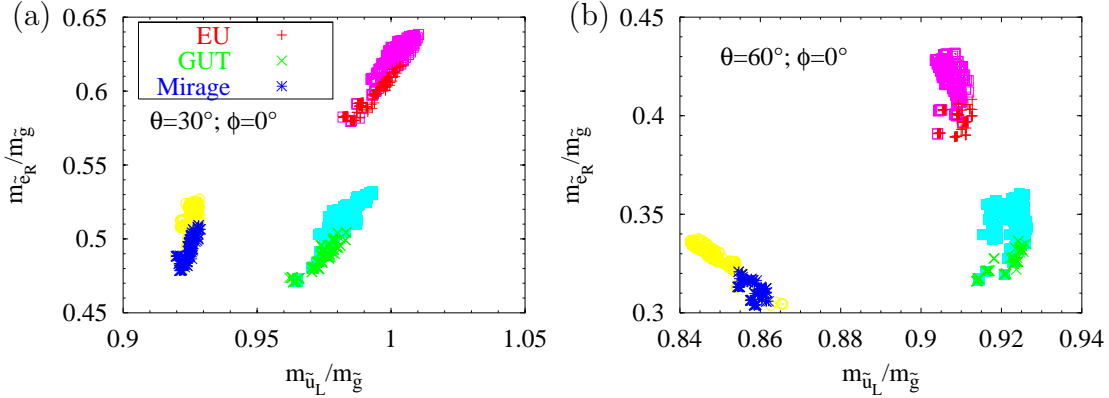


**Figure 9:** Discriminating ratios of sparticle masses in departures from dilaton domination: (a)  $\theta = 30^\circ, \phi = 0^\circ$  and (b)  $\theta = 60^\circ, \phi = 0^\circ$ . Each plotted point corresponds to one  $(m_{3/2}, \tan \beta)$  pair in the scan not excluded by the limits. Green crosses are predicted by the GUT unification scale, early unification is denoted by red crosses, and blue stars are valid for the mirage unification scenario.  $g - 2$  limits have not been applied to the yellow circles (mirage unification), purple squares (early unification) and cyan squares (GUT-scale unification).

figures 9a-9b show, however, that the required accuracy on the ratios  $m_{\tilde{u}_L}/m_{\tilde{g}}$  and  $m_{\tilde{e}_R}/m_{\tilde{g}}$  is approximately constant with respect to a variation of the goldstino angles. From figures 9a,b we see that for  $\theta = 30^\circ, \phi = 0^\circ$  or  $\theta = 60^\circ, \phi = 0^\circ$ , a 6% measurement of  $m_{\tilde{u}_L}/m_{\tilde{g}}$  and a 5% measurement of  $m_{\tilde{e}_R}/m_{\tilde{g}}$  would discriminate the scenarios. In fact, these ratios discriminate the scenarios for any fixed value of  $\theta, \phi$  but do not completely discriminate once the goldstino angles are scanned over. It is therefore difficult to say much that is definitive about the ratios in this case. It is possible that specific models will predict the goldstino angles, and in that case the two ratios mentioned above will be useful. However, the connection between measured quantities and  $\theta, \phi$  is perhaps less obvious than for  $m_{3/2}$  and  $\tan \beta$ . This means that it is difficult to see how one would directly infer their values from experimental data, and so we leave the discussion of constrained goldstino angles here.

### 3.6 Interpretation

Note that the required accuracy quoted here is the one necessary to separate the closest two points between different scenarios. This is the most pessimistic scenario, and we may well require less accuracy depending upon where the data finally lie. For example figure 6c shows that the data  $m_{\tilde{d}_L}/m_{\tilde{e}_R} \sim 3.1 \pm 0.6$  and  $m_{\tilde{g}}/m_{\tilde{u}_L} \sim 1.10 \pm 0.03$ , would imply that the GUT-scale scenario would be selected over the other two whereas for  $m_{\tilde{d}_L}/m_{\tilde{e}_R} \sim 1.8$  and  $m_{\tilde{g}}/m_{\tilde{u}_L} \sim 1.0$ , uncertainties of  $(0.2, 0.02)$  would be required respectively. Where the data finally lie will also decide the most important measurement. We take the dilaton dominated scenario to exemplify this

point (see figure 7). If the data lie over the GUT-scale region, the most important errors are those upon  $m_{\tilde{e}_L}/m_{\tilde{e}_R}$  as this will best separate the GUT-scale scenario from the other two. If, on the other hand, the data lie over the early unification scenario, it is more important to have smaller uncertainties upon  $m_{\tilde{g}}/m_{\tilde{u}_L}$  for discrimination.

We must ask what effect theoretical errors have on the interpretation of the results. Comparisons between the spectra derived from SOFTSUSY [20] code and ISASUGRA [14], while showing qualitative agreement, display differences of order of the mass differences required to discriminate the scenarios [21, 20]. The errors are both dependent upon the flavour of particle (sleptons tend to have very good agreement, whereas coloured objects typically show a 3-5% difference) and on the region of parameter space. For extreme places in parameter space, for example near the radiative electroweak symmetry breaking boundary, predicted mass differences can be large between the two codes [21, 20]. However, provided the point in parameter space being examined is not particularly special, any theoretical errors in codes should not change our conclusions about discrimination. This is because the errors due to (for example) not including finite threshold corrections in ISASUGRA will affect all points in the three scenarios in roughly the same way, moving them all in one direction for example.

It is clear, however, that better accuracy in the mass predictions will be necessary when interpreting real data. Of course, the discrimination depends at face value on the assumption of prior knowledge either of the goldstino angles (which will probably not be owned) or of  $m_{3/2}$  and  $\tan\beta$ . The latter pair of parameters may be predicted in the hypothesis of each scenario, since gaugino masses that can help set  $m_{3/2}$  and  $\tan\beta$  may well be obtained from Higgs measurements [22]. We note that each discriminating plot is valid for two particular values of fixed parameters. If the fixed parameters are not determined beforehand, they would have to be fit to the sparticle masses. This fitting procedure will be subject more to the theoretical errors, and will require them to be shrunk from their current levels. We would of course use all available (*i.e.* measured) highly discriminating ratios simultaneously in order to try to pin down the correct scenario. This would provide additional confirmation that the identified scenario is the correct one.

edge variable	accuracy
$m_{\tilde{u}}^{\max}$	0.1%
$m_{\tilde{u}q}^{\max}$	1%
$m_{\tilde{t}q(\text{low})}$	1%

**Table 2:** Accuracy of most useful LHC edge variables.

It is likely that the next machine capable of producing TeV-scale superparticles in sufficient numbers to make a reasonable measurement is the LHC. It remains to be seen how good the LHC is in determining ratios of masses, but it cannot constrain any single sparticle mass to a very accurate level (10% or so on the absolute values). The LHC can however constrain certain functions of masses to about 1% [23, 6, 24] by finding the end-points of kinematic distributions. In ref. [24], the three most accurate measurements were found to be on the edges in the invariant masses detailed in

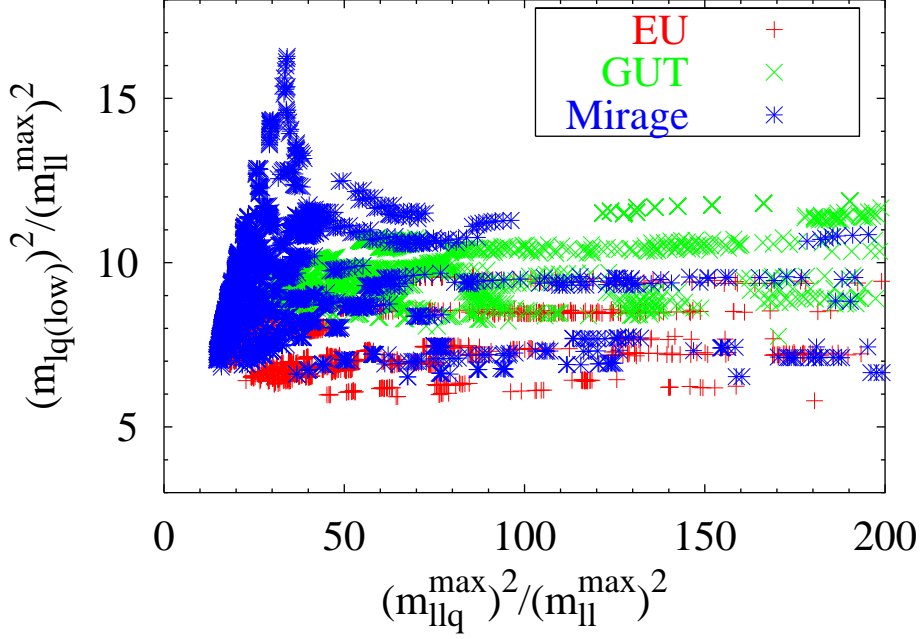


**Figure 10:** Ratios of LHC edge variables. Each plotted point corresponds to one data point in four-dimensional parameter space  $(\theta, \phi, \tan\beta, m_{3/2})$  that is not excluded by the imposed limits and where  $m_{\chi_2^0} > m_{\tilde{l}_R}$ .

table 2. They follow parts of the decay chain of  $\tilde{q} \rightarrow q\chi_2^0$ ,  $\chi_2^0 \rightarrow \tilde{l}\tilde{l}$  then  $\tilde{l} \rightarrow l\chi_1^0$ . The existence of this chain depends upon the mass ordering  $m_{\tilde{q}} > m_{\chi_2^0} > m_{\tilde{l}}$ .

The edges shown in table 2 measure [24]

$$\begin{aligned}
(m_{ll}^{\max})^2 &= \frac{(m_{\chi_2^0}^2 - m_{\tilde{l}_R}^2)(m_{\tilde{l}_R}^2 - m_{\chi_1^0}^2)}{m_{\tilde{l}_R}^2}, \\
(m_{lq(\text{low})})^2 &= \min \left[ \frac{(m_{\tilde{q}}^2 - m_{\chi_2^0}^2)(m_{\chi_2^0}^2 - m_{\tilde{l}_R}^2)}{m_{\chi_2^0}^2}, \frac{(m_{\tilde{q}}^2 - m_{\chi_2^0}^2)(m_{\tilde{l}_R}^2 - m_{\chi_1^0}^2)}{2m_{\tilde{l}_R}^2 - m_{\chi_1^0}^2} \right], \\
(m_{llq}^{\max})^2 &= \max \left[ \frac{(m_{\tilde{q}}^2 - m_{\chi_2^0}^2)(m_{\chi_2^0}^2 - m_{\chi_1^0}^2)}{m_{\chi_2^0}^2}, \frac{(m_{\tilde{q}}^2 - m_{\tilde{l}_R}^2)(m_{\tilde{l}_R}^2 - m_{\chi_1^0}^2)}{m_{\tilde{l}_R}^2}, \right. \\
&\quad \left. \frac{(m_{\tilde{l}_R}^2 m_{\tilde{q}}^2 - m_{\chi_1^0}^2 m_{\chi_2^0}^2)(m_{\chi_2^0}^2 - m_{\tilde{l}_R}^2)}{m_{\tilde{l}_R}^2 m_{\chi_2^0}^2} \right], \tag{3.6}
\end{aligned}$$

except for the special case in which  $m_{\tilde{l}_R}^4 < m_{\tilde{q}}^2 m_{\chi_1^0}^2 < m_{\chi_2^0}^4$  and  $m_{\chi_2^0}^4 m_{\chi_1^0}^2 < m_{\tilde{q}}^2 m_{\tilde{l}_R}^4$  when  $(m_{llq}^{\max})^2 = (m_{\tilde{q}} - m_{\chi_1^0})^2$  instead. We use  $m_{ll}^{\max}$  to normalise the other edge variables, as its small error is negligible. We therefore plot the ratios  $(m_{llq}^{\max})^2 / (m_{ll}^{\max})^2$  against  $(m_{lq(\text{low})})^2 / (m_{ll}^{\max})^2$  in figure 10 in order to see if these precision LHC measurements can be used to distinguish the string scenarios. All four free parameters are scanned over and all current experimental constraints (including  $g - 2$  of the muon) are

applied. Additionally, we require  $m_{\chi_2^0} > m_{\tilde{l}_R}$ , to make sure that the above mentioned decay chain actually exists. This is the case in roughly one third of the investigated parameter space. The maximum value in the  $(m_{\tilde{l}q}^{\max})^2/(m_{\tilde{l}}^{\max})^2$  direction depends strongly on the mass difference between  $\tilde{l}_R$  and  $\chi_2^0$ . As they approach degeneracy,  $(m_{\tilde{l}q}^{\max})^2/m_{\tilde{l}}^{\max}$  can get as large as  $10^5$ .

As figure 10 shows, there is no clear separation between all scenarios on the basis of these LHC edge variables. However, the  $(m_{lq(\text{low})})^2/(m_{\tilde{l}}^{\max})^2$ -axis provides some exclusion limits: only in the mirage case, for example, can one obtain values  $> 12$ . Similarly, the GUT scale case could be ruled out if  $(m_{lq(\text{low})})^2/(m_{\tilde{l}}^{\max})^2 < 8$ . If the horizontal axis could be replaced with an observable that shows similar properties, the distinction would become better.

## 4. Conclusions

We have seen that general information can be obtained about string theory scenarios. We considered three general string scenarios: two with the MSSM superfield content (GUT scale unification and mirage unification at the intermediate scale) and one with additional leptons and unification at the intermediate scale. We have mapped out the available parameter space for each scenario, using current empirical constraints.

Our main results are better summarized in figures 3 and 6. From figure 3 we were able to extract general limits on the values of the gravitino mass and  $\tan\beta$  for each of the three scenarios. We can see clearly that for different combinations of values of the goldstino angles only a limited region of  $m_{3/2} - \tan\beta$  parameter space is allowed, and therefore a maximum value for each of them can be extracted.

In figure 6 we find, quite remarkably, that ratios of particle masses are able to completely separate each scenario when *all* parameters:  $\theta, \phi, m_{3/2}, \tan\beta$  are considered. This allows us to differentiate between the three scenarios. Clearly, fixing some of the parameters makes the separation between scenarios cleaner (see figs. 7-9). We then determined what accuracy is required on the measurement of these masses in order to distinguish the scenarios. The errors are required to be less than the few percent level, depending upon the exact ratio.

A previous study [25] found that the exotic heavy leptons present in the early unification scenario, can be discovered by the LHC if their masses are less than 980 GeV. This could confirm the mirage scenario, making further discrimination redundant between the models considered here. The exotic leptons would not be discovered if they were heavier than 1 TeV, so all three scenarios would still be left to be distinguished in that case. We note that a previous study confronted a fundamental SUGRA model with detailed linear collider and LHC measurements in a bottom-up approach [26]. Presumably, this kind of analysis could be repeated for stringy scenarios and would complement the present study. It could be used to provide accurate

	$\tilde{g}$	$m_{\tilde{e}_R}$	$m_{\tilde{e}_L}$	$m_{\tilde{u}_L}$	$m_{\tilde{t}_1}$	$m_{\tilde{t}_2}$	$M_{\tilde{\chi}_1^0}$	$m_{H^0, A^0}$
Early	0.4-1.6	0.1-0.9	0.2-1.0	0.4-1.5	0.2-1.1	0.4-1.3	0.1-0.4	0.2-0.7
Mirage	0.5-2.0	0.1-0.9	0.2-0.9	0.4-1.7	0.3-1.4	0.5-1.6	0.1-0.5	0.2-0.8
GUT	0.4-1.7	0.1-0.8	0.2-0.9	0.4-1.6	0.2-1.2	0.4-1.4	0.0-0.4	0.2-0.9

**Table 3:** Range of relevant sparticle masses coming from the parameter scans, in TeV.  $2\sigma$  limits on  $g-2$  of the muon have been imposed. The rows are marked by string scenario: early unification, mirage and GUT-scale unification respectively.

measurements of high-scale soft-breaking parameters and to determine at what scale they unify.

The small percent-level errors required on mass ratios are not expected to occur at the Tevatron experiments [27], or even at the LHC [6]. But it is likely that a future linear  $e^+e^-$  collider facility [22] would have sufficient accuracy, provided it had sufficient centre of mass energy to produce some of the particles involved in the ratios. For this reason, we present the ranges of relevant sparticle masses in table 3. The upper limit on these ranges are critically dependent on the maximum scanned values of  $m_{3/2}$  and  $\tan\beta$ . It is clear that for these maximum scanned values, only a multi TeV facility such as CLIC would provide enough centre of mass energy to cover the entire range. We note, however, that lower values of  $m_{3/2}$  are favoured by the fine-tuning parameter [7], and so the mass ranges shown in table 3 might be too pessimistic.

Also we were able to extract general information on limits on gravitino mass and constraints on possible values of  $\tan\beta$ . The use of the muon anomalous magnetic moment information may be read in two ways. First, assuming that the current experimental results continue to hold, we have a constraint on our parameters (even if the effect should go away, significant constraints still persist in the  $\tan\beta$  direction from CLSP considerations). Second, for fixed goldstino angles we may extract the maximum contribution to the muon  $g-2$  coming from these scenarios. This information may be relevant once experimental statistics are improved.

There are several directions in which our work can be extended. First we may incorporate the charge and colour breaking (CCB) constraints on all the scenarios, as was done for the dilaton domination scenario in ref. [7]. While it would certainly be interesting to know if the universe were in some meta-stable vacuum, a global CCB vacuum might not necessarily rule the model out [28]. We could impose some arbitrary fine-tuning constraint on the models in order to restrict the maximum values of  $m_{3/2}$ ; this would presumably increase the discriminatory power of our mass ratio tests. Another extension relates to the consideration of moduli domination, a limit that we did not consider since in that case the soft breaking terms appear only at the loop level and therefore anomaly mediation cannot be neglected. It is an open question to correctly combine anomaly mediation with gravity mediation for all soft

breaking terms.

This study is a first step towards the experimental discrimination of string models, leaving plenty of room for more investigation. For example, it would be interesting to know the search reach in parameter space of the various future colliders as could be performed by HERWIG [29]. Further, we would like to know under which conditions experiments will be able to measure the discriminatory mass ratios.

We hope that the techniques introduced in this article can be used to discriminate other SUSY breaking scenarios, assuming eventual discovery of supersymmetric particles.

## Acknowledgments

This work is funded by the Studienstiftung des deutschen Volkes and the UK Particle Physics and Astronomy Research Council (PPARC). DG and FQ thank CERN Theory division for their hospitality. DG thanks H Baer for advice on the ISASUGRA package. BCA thanks J Ellis for providing inspiration and we would all like to thank members of the Cambridge LHC SUSY working group for interesting discussions on more experimental aspects.

## References

- [1] E. Witten, *Strong Coupling Expansion Of Calabi-Yau Compactification*, *Nucl. Phys.* **B 471** (1996) 135, [[hep-th/9602070](#)].
- [2] K. Benakli, *Phenomenology of Low Quantum Gravity Scale Models*, *Phys. Rev.* **D 60** (1999) 104002, [[hep-ph/9809582](#)].
- [3] C. P. Burgess, L. E. Ibáñez and F. Quevedo, *Strings at the Intermediate Scale, or is the Fermi Scale Dual to the Planck Scale?*, *Phys. Lett.* **B 447** (1999) 257, [[hep-ph/9810535](#)].
- [4] G. Aldazabal, L. E. Ibáñez and F. Quevedo, *Standard-like models with broken supersymmetry from type I string vacua*, *J. High Energy Phys.* **01** (2000) 031, [[hep-th/9909172](#)]; *A D-brane alternative to the MSSM*, *J. High Energy Phys.* **0002** (2000) 015 [[hep-ph/0001083](#)]. D. Bailin, G. V. Kraniotis and A. Love, *Supersymmetric standard models on D-branes*, *Phys. Lett. B* **502**, 209 (2001) [[hep-th/0011289](#)]; G. Aldazabal, L. E. Ibáñez, F. Quevedo and A. M. Uranga, *D-branes at singularities: A bottom-up approach to the string embedding of the standard model*, *J. High Energy Phys.* **0008** (2000) 002 [[hep-th/0005067](#)].
- [5] L. E. Ibáñez, *Mirage gauge coupling unification*, [[hep-ph/9905349](#)].
- [6] ATLAS collaboration, *ATLAS Detector and Physics Performance Technical Design Report*, CERN/LHCC/99-15, ATLAS TDR 14, 25 May 1999.

- [7] S. A. Abel, B. C. Allanach, L. E. Ibáñez, M. Klein and F. Quevedo, *Soft SUSY Breaking, Dilaton Domination and Intermediate Scale String Models*, *J. High Energy Phys.* **12** (2000) 026, [[hep-ph/0005260](#)]; S. A. Abel and B. C. Allanach, *Quasi-Fixed Points and Charge and Colour Breaking in Low Scale Models*, *J. High Energy Phys.* **07** (2000) 037, [[hep-ph/9909448](#)].
- [8] S. Baek, P. Ko and H. S. Lee, *Muon anomalous magnetic moment,  $B \rightarrow X/s$  gamma and dark matter detection in the string models with dilaton domination*, [[hep-ph/0103218](#)]; D. G. Cerdeño, E. Gabrielli, S. Khalil, C. Muñoz and E. Torrente-Lujan, *Muon anomalous magnetic moment in supersymmetric scenarios with an intermediate scale and nonuniversality*, [[hep-ph/0104242](#)].
- [9] D. Bailin, G. V. Kraniotis and A. Love, *Sparticle spectrum and dark matter in type I string theory with an intermediate scale*, *Phys. Lett.* **B 491** (2000) 161, [[hep-ph/0007206](#)];
- [10] E. Gabrielli, S. Khalil, C. Muñoz and E. Torrente-Lujan, *Initial scales, supersymmetric dark matter and variations of neutralino nucleon cross sections*, *Phys. Rev.* **D 63** (2001) 025008, [[hep-ph/0006266](#)]; D. G. Cerdeño, E. Gabrielli, S. Khalil, C. Muñoz and E. Torrente-Lujan, *Determination of the string scale in D-brane scenarios and dark matter implications*, *Nucl. Phys.* **B 603** (2001) 231, [[hep-ph/0102270](#)].
- [11] J. A. Casas, A. Ibarra and C. Muñoz, *Phenomenological viability of string and M-theory scenarios*, *Nucl. Phys.* **B 554** (1999) 67 [[hep-ph/9810266](#)].
- [12] A. Brignole, L. E. Ibáñez and C. Muñoz, *Towards a Theory of Soft Terms for the Supersymmetric Standard Model*, *Nucl. Phys.* **B 422** (1994) 125, [[hep-ph/9308271](#)].
- [13] J. A. Bagger, T. Moroi and E. Poppitz, *Anomaly mediation in supergravity theories*, *J. High Energy Phys.* **04** (2000) 009, [[hep-th/9911029](#)].
- [14] H. Baer, F. E. Paige, S. D. Protopopescu and X. Tata, *ISAJET 7.48: A Monte Carlo Event Generator for  $pp$ ,  $\bar{p}p$ , and  $e^+e^-$  Interactions*, [[hep-ph/0001086](#)].
- [15] Particle Data Group, *Review of Particle Properties*, *Eur. Phys. Jour.* **C15** (2000) 1, and 2001 partial update for the 2002 edition available on the PDG WWW pages (URL: <http://pdg.lbl.gov/>).
- [16] H. N. Brown *et al.*, Muon  $g - 2$  Collaboration, *Precise measurement of the positive muon anomalous magnetic moment*, *Phys. Rev. Lett.* **86** (2001) 2227, [[hep-ex/0102017](#)].
- [17] A. Czarnecki and W. J. Marciano, *The muon anomalous magnetic moment: A harbinger for new physics*, *Phys. Rev.* **D 64** (2001) 013014, [[hep-ph/0102122](#)].
- [18] See for instance: S. P. Martin and J. D. Wells, *Muon anomalous magnetic dipole moment in supersymmetric theories*, *Phys. Rev.* **D 64** (2001) 035003, [[hep-ph/0103067](#)] and references therein.



- [19] G. Aldazabal, L. E. Ibáñez and F. Quevedo, *A D-Brane Alternative to the MSSM*, *J. High Energy Phys.* **02** (2000) 015, [[hep-ph/0001083](#)].
- [20] B. C. Allanach, *SOFTSUSY: a program for calculating supersymmetric spectra*, [[hep-ph/0104145](#)].
- [21] B. C. Allanach, *Theoretical Uncertainties in Sparticle Mass Predictions*, P3-19 preprint of Snowmass **2001** conference, CERN-TH/2001-255, [[hep-ph/0110227](#)].
- [22] J. A. Aguilar-Saavedra *et al.* ECFA/DESY LC Physics Working Group Collaboration, *TESLA Technical Design Report Part III: Physics at an e+e- Linear Collider*, [[hep-ph/0106315](#)].
- [23] J. G. Branson *et al.*, *High transverse momentum physics at the Large Hadron Collider*, [[hep-ph/0110021](#)].
- [24] B. C. Allanach, C. G. Lester, M. A. Parker and B. R. Webber, *Measuring sparticle masses in non-universal string inspired models at the LHC*, *J. High Energy Phys.* **09** (2000) 004, [[hep-ph/0007009](#)].
- [25] B.C. Allanach *et al.*, *Detecting Exotic Heavy Leptons at the Large Hadron Collider*, *J. High Energy Phys.* **08** (2001) 051, [[hep-ph/0108097](#)].
- [26] G. A. Blair, W. Porod and P. M. Zerwas, *Reconstructing supersymmetric theories at high energy scales*, *Phys. Rev. D* **63** (2001) 017703, [[hep-ph/0007107](#)].
- [27] S. Abel *et al.* SUGRA Working Group Collaboration, *Report of the SUGRA working group for run II of the Tevatron*, [[hep-ph/0003154](#)].
- [28] S.A. Abel and C.A. Savoy, *On metastability in supersymmetric models*, *Nucl. Phys. B* **532** (1998) 3, [[hep-ph/9803218](#)].
- [29] G. Corcella *et al.*, *HERWIG 6.1 Release Note*, [hep-ph/9912396](#); G. Corcella *et al.*, *HERWIG 6: an event generator for Hadron Emission Reactions With Interfering Gluons (including supersymmetric processes)*, *J. High Energy Phys.* **01** (2001) 010, [[hep-ph/0011363](#)].